Correlation between nanoscale and nanosecond resolved ferroelectric domain dynamics and local mechanical compliance

N. A. Polomoff, A. Rakin, S. Lee, V. Palumbo, P. Yu, Y. H. Chu, R. Ramesh, and B. D. Huey

Citation: Journal of Applied Physics **109**, 091607 (2011); doi: 10.1063/1.3581205
View online: http://dx.doi.org/10.1063/1.3581205
View Table of Contents: http://scitation.aip.org/content/aip/journal/jap/109/9?ver=pdfcov
Published by the AIP Publishing

Correlation between nanoscale and nanosecond resolved ferroelectric domain dynamics and local mechanical compliance

N. A. Polomoff,[1] A. Rakin,[1] S. Lee,[1,2] V. Palumbo,[1] P. Yu,[3] Y. H. Chu,[4] R. Ramesh,[3] and B. D. Huey[1,a)]

[1]*Institute of Materials Science, University of Connecticut, Storrs, Connecticut 06269, USA*
[2]*Division of Physical Metrology, Korea Research Institute of Standards and Science, Daejeon 305-340, South Korea*
[3]*Department of Physics, University of California at Berkeley, Berkeley, California 94720, USA*
[4]*Department of Materials Science and Engineering, National Chiao Tung University, HsinChu 300, Taiwan*

(Received 5 March 2010; accepted 25 June 2010; published online 13 May 2011)

The local dynamics of ferroelectric domain polarization are uniquely investigated with sub-20-nm resolved maps of switching times, growth velocities, and growth directions. This is achieved by analyzing movies of hundreds of consecutive high speed piezo force microscopy images, which record domain switching dynamics through repeatedly alternating between high speed domain imaging and the application of 20-nanosecond voltage pulses. Recurrent switching patterns are revealed, and domain wall velocities for nascent domains are uniquely reported to be up to four times faster than for mature domains with radii greater than approximately 100 nm. Switching times, speeds, and directions are also shown to correlate with local mechanical compliance, with domains preferentially nucleating and growing in compliant sample regions while clearly shunting around locations with higher stiffness. This deterministic switching behavior strongly supports a defect-mediated energy landscape which controls polarization reversal, and that can therefore be predicted, modeled, and even manipulated through composition, processing, and geometry. Such results have important implications for the practical performance of ferroelectric devices by enabling guided optimization of switching times and feature densities, while the methods employed provide a new means to investigate and correlate dynamic functionality with mechanical properties at the nanoscale. © *2011 American Institute of Physics*. [doi:10.1063/1.3581205]

I. INTRODUCTION

There are a wide variety of applications for ferroelectric thin films, including nonvolatile memory devices, frequency agile tunable filters, infrastructure health monitoring, thermal management systems, etc. Polarization switching has received particular attention with the development and widespread use of piezo force microscopy (PFM)[1], allowing spatially and temporally resolved dynamics investigations of domain switching, growth, or relaxation[2–7] which lately have leveraged pulsing or pump:probe schemes[8,9] and/or high speed scanning capabilities[10,11] that even allow polarization mapping during actual switching.[12–14] This paper extends such switching dynamics studies into a new area: investigating nascent nucleation and growth dynamics along with their correlation to local mechanical properties.

For domain imaging using standard PFM, an AC dither bias is applied to a ferroelectric sample, causing normal and/or lateral vibrations of the surface due to the converse piezoelectric effect. The resulting picometer-scale vibrations are detectible by atomic force microscopy (AFM) leveraging lock-in techniques, providing nanometer scale spatial resolution of the local piezoresponse. The measured amplitude is indicative of the local piezoelectric coefficients, while the phase identifies the domain orientation. For the work described here, the biasing is supplied directly to a conducting AFM probe contacting the exposed surface of a ferroelectric (PZT) thin film. The samples are grown epitaxially onto a (001) $SrTiO_3$ substrate with an intermediate $SrRuO_3$ conducting electrode film, fabricated by pulsed laser deposition as previously described.[15]

In order to directly monitor domain switching with PFM during *in situ* poling, the AC dither bias for domain orientation imaging (usually 1–3 V amplitude) is also superimposed with a constant DC offset for poling (typically 0 to ±4 V).[12] Whenever the electric field from this combined signal surpasses the film's coercive field ($\pm E_c$), ferroelectric switching may progress between the possible polarization states. For the strained epitaxial film considered here, only states into and out of the plane are observed; 90° in-plane domains are not found. In any case, since any poling is localized beneath the scanned probe, while the rest of the sample is not exposed to appreciable biasing, the poling time per imaged pixel is a function of the resident time the biased nanoscale AFM tip interacts with any given pixel. Finally, as the ferroelectric domain configuration is stable after each image, literally for years, repeatedly imaging a given area essentially yields 'stop-motion' movies of the switching process for cumulatively longer switching times, while maintaining high temporal resolution dependent upon the poling time per individual pixel. This approach is especially suited to high speed PFM (HSPFM) measurements, where significantly higher line scanning rates are employed than standard AFM or

a)Author to whom correspondence should be addressed. Electronic mail: bhuey@ims.uconn.edu.

PFM, and therefore numerous images (time steps) can be efficiently acquired.[12]

II. EXPERIMENTAL

A 40 Hz scanning rate is utilized for all HSPFM images presented herein, generating a new image every 6.4 s. Temporal resolution of several microseconds per pixel per image frame has thus been achieved during HSPFM with a continuous AC + DC bias applied,[12] while 10 ns temporal resolution is achieved by applying individual pulses per pixel in a pump:probe configuration.[16] This work was performed on Asylum Research MFP-3d and Cypher systems, with a SRS lock-in amplifier (model 844) for piezoresponse amplitude and phase detection. The voltage signals are supplied by an Agilent function generator (33250a) to the Nanoworld conducting AFM probe (DESP). Experiments are automated and data recorded with Agilent Vee software and a Measurement Computing high speed data acquisition card (DAS-4020).

III. DETERMINISTIC NUCLEATION AND GROWTH

This work is motivated by high speed PFM results for repeated poling of a given area, for which the nucleation and growth pattern is reproducible with each switching event.[13] As an example, Fig. 1 presents 23 HSPFM phase images from a movie of 115 consecutively acquired frames (every 4th is shown, with the full HSPFM phase and amplitude movies available online as supplemental material, Figs. S1a and S1b, respectively).[17] Each image displays the domain configuration for the same $2 \times 2\ \mu m^2$ area during repeated switching with the continual application of AC and DC biases, where contrast in the phase images indicates domain orientation (001 or 00-1). In the first frame 0 V of DC bias are applied, revealing a uniformly poled region. The next frame, with a light arrow pointing right, indicates the first of 5 images where the extreme of the applied bias (−5 V) extends below the negative coercive field ($-E_c$), as identified in the sketch at lower right. Clearly, dark domains appear, with roughly 40 initial nucleation sites in the imaged area that appear and grow with further biasing following distinct patterns. For the next 3 frames, beginning with the dark arrow, the positive coercive field is addressed ($+E_c$) with a maximum of +1.7 V, again as sketched at lower right, returning the polarity to the opposite orientation (light contrast) for nearly the entire imaged area. This cycle is then repeated, with negative fields applied for frames 10–12, positive from 13–15, negative from 16–18, positive from 19–21, and finally negative for 22–23. The distribution and order of appearance for nucleation sites, as well as the growth directions and velocities of the domain walls, are largely repeatable, highlighted by the circled features in frames 4, 12, 18, and 23.

Focusing on individual nucleation sites further, higher temporal resolution studies were conducted with a pump:probe variation of HSPFM.[16] As sketched in Fig. 2(a), during one pass of the tip over the sample, individual pulses are applied to the tip at each pixel with pulse durations down to 20 ns. During the next pass, a small AC signal is applied only to the tip to map the resulting domain configuration. This process is then repeated as often as necessary to switch an area of interest, resulting in consecutive images of the progressive domain patterns as sketched by contrast [Fig. 2(b)]. Similar measurements have been reported elsewhere using standard speed PFM, but typically with increasing pulse

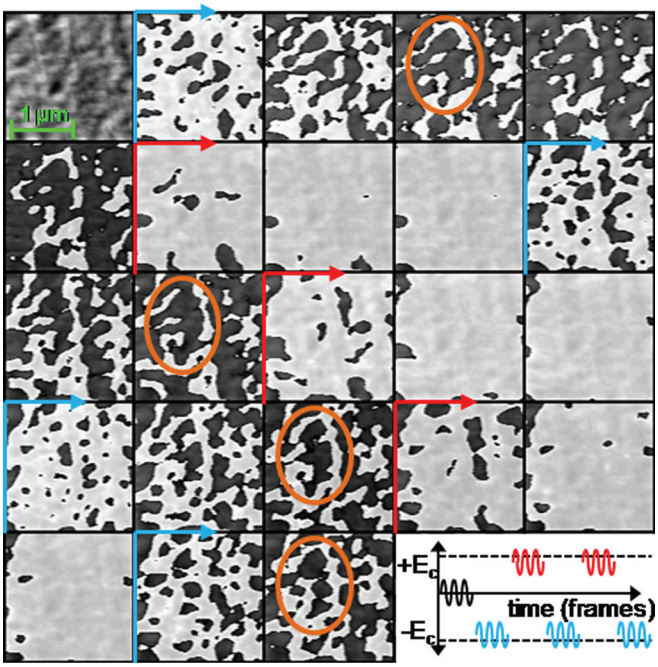

FIG. 1. (Color online) Progressive HSPFM images of a single $2 \times 2\ \mu m^2$ area, with sufficient bias applied to pole domains from one polarity, back to the other, and back again repeatedly, revealing predictable domain nucleation and growth patterns.

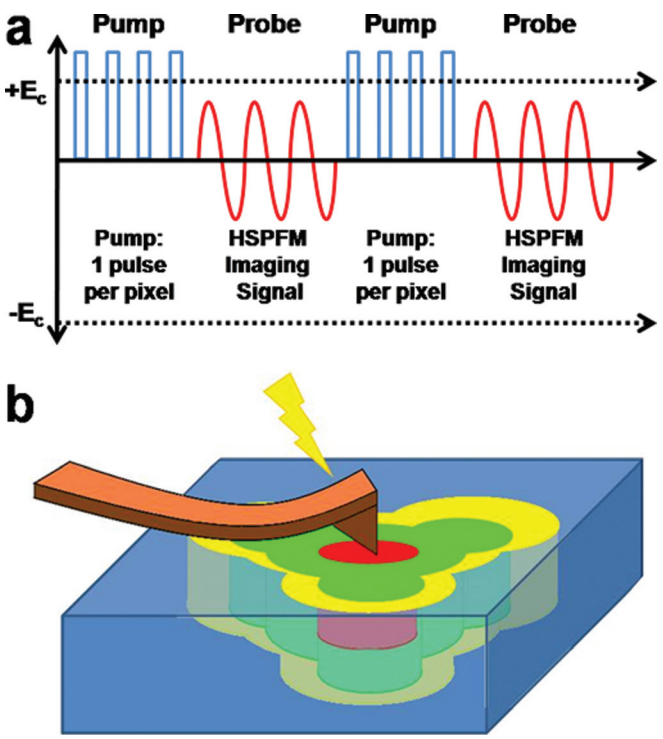

FIG. 2. (Color online) Sketch of pump:probe configured HSPFM for sequential pulsing and ferroelectric domain imaging (a) in order to monitor progressive domain growth with increasing cumulative switching times (b).

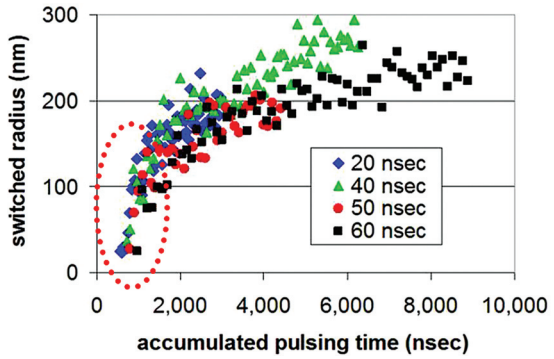

FIG. 3. (Color online) Radius of a single domain during switching as a function of accumulated pulse time, poled and repoled 4 times for pulses of increasing durations, exhibiting consistently accelerated growth velocities for the nascent domain up to a radius of approximately 125 nm (circled). Reprinted with permission from N. A. Polomoff, R. N. Premnath, J. L. Bosse, and B. D. Huey, J. Mater. Sci. 44, 5189 (2009). Copyright © 2009, Springerlink

durations for each successive frame in order to monitor complete switching in a manageable experimental time frame.[9,18] Since high speed PFM is employed here, where image rates of a few seconds per frame or faster are standard,[12] constant pulse widths can be reasonably employed instead. This yields switching movies of hundreds of image frames, requiring only minutes to tens of minutes to acquire, yet subtleties in the nucleation and growth behavior can be uniquely monitored throughout the entire switching process by maintaining constantly high spatial and temporal resolution.

Accordingly, Fig. 3 tracks the domain radius of a single domain as a function of accumulated pulse time, for various pulse durations. The radius is determined based on the domain area, or equivalently domain perimeter, each of which is easily calculated automatically using standard image analysis tools (ImageJ, Improvision Volocity) employing simple light/dark contrast thresholds. Although the linear growth beyond switching times of roughly 2 μs was previously reported (see[16] for the entire switching movie), an apparently enhanced growth rate for nascent domains was not previously noted. In this case, the domain radius expands with an initially high velocity of 0.34 m/sec up to a radius of approximately 125 nm, beyond which the slope slows to roughly 0.14 m/sec, with linear growth for many microseconds until the domain converges with another.

Combining the observations from Figs. 1 and 3, it is clear that both domain nucleation and growth are deterministic, domain growth is rapid to a certain critical radius, and beyond that radius the domain growth slows to a seemingly constant velocity. Similar measurements on numerous other domains reveal an equivalent response, though with varying nucleation times, initial and final growth velocities, and critical radii. We have separately proven that domain nucleation times and their eventual linear growth rates are uncorrelated,[13] and as noted elsewhere they are exponentially related to the applied voltage.[11,14] Finally, even though on average the domain radii expand smoothly, locally the domain wall velocities and directions clearly vary deterministically with position (e.g., Figure 1). Such directionality for domain growth has separately been correlated to particular crystal directions.[2,7,19,20] These observations provide strong evidence for: (i) the presence of a dominant defect at the nucleation site with an activation energy barrier for domain switching that is diminished compared to the surrounding film; (ii) a short range influence by this defect on domain growth, to a distance on the order of 100 nm or less; and (iii) growth beyond this radius unimpeded by the initiating defect, determined instead by the surrounding energy landscape.[8,13,20]

Once a domain has nucleated at a low activation energy defect site, during further poling the advancing domain wall should thus encounter a distribution of activation energies from the various defects that may exist at the domain periphery, locally enhancing or retarding growth in specific directions. Consequently, as dimensions continue to shrink for ferroelectric devices that leverage polarization switching, the performance of those devices will crucially depend on being able to predict and/or control such nucleation and growth behavior. The remainder of this work leverages nanosecond pulsing with pump-probe HSPFM to uniquely focus on nanoscale domain growth directions and velocities, especially their correlation to measureable film defects which influence the energy landscape and hence the overall switching dynamics.

IV. AVERAGE DOMAIN DYNAMICS

With this in mind, a 2×2 μm^2 region from the same PZT film as considered in Fig. 1 was repeatedly imaged with pump:probe HSPFM as described in Fig. 2. We acquired 152 consecutive images in this manner, between which pulses with amplitudes of 2 V and durations of 20 ns were applied to each image pixel. As before, the entire switching movie, both for phase and amplitude contrast, is available as supplementary online content (Figs. S4a and S4b).[17] Figure 4 presents essentially the same result, but with 60 ns of accumulated pulsing separating each progressive domain orientation (HSPFM phase) image (i.e., only every third frame is shown for brevity). One domain at the lower right is particularly highlighted by contrast for the ensuing discussion, and a solid square region and a dotted rectangular region are both outlined for further consideration at higher magnification. The final image frame displays the topography for the same area, acquired at a standard (1 Hz) imaging rate, with a total contrast range (black to white) of just ± 1 nm. The area is extraordinarily flat, with <400 pm RMS roughness, with a predominant protrusion at lower right extending 2 nm above the surface plane, another smaller $+1$ nm protrusion at nearly the exact center of the image, and a 1.4 nm step running at roughly 45° from upper right to lower left that is likely related to an atomic step on the vicinal substrate upon which the film is epitaxially grown.

The progressive areas during switching of all domains in each frame of Fig. 4 were automatically tracked as discussed elsewhere.[14,21] Figure 5 particularly plots the radius of the highlighted domain as a function of poling time (left axis), superimposed with the percent switched area for the entire image region (right axis). This overall switched area obeys an 'S-curve' relationship as discussed elsewhere, though the

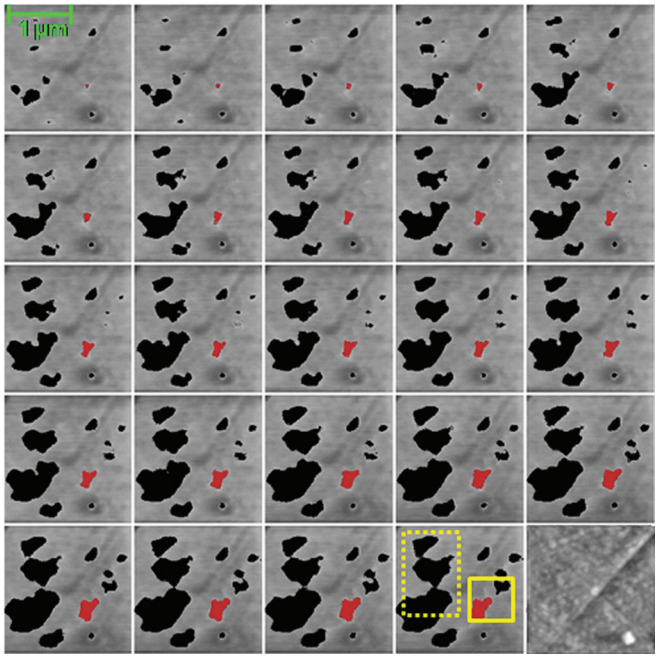

FIG. 4. (Color online) Montage of 24 progressive phase images from a movie of 152 pump:probe HSPFM frames during polarization switching of a 2×2 μm^2 area, revealing domain orientation by contrast with 60 ns of cumulative poling time per pixel between each image. The image at lower right indicates the topography for the same region, with a total contrast range of ± 1.5 nm.

poling experiment is terminated long before 100% completion. The response for the single domain, on the other hand, is roughly linear, though the high temporal resolution employed here reveals occasional changes in the slope (two are circled), sometimes with accelerated growth, sometimes hindered. A similar behavior is apparent for most other domains in the switching movie as well. Note that the image frames in Fig. 4, upon which the single domain data are based, span only a small fraction of the overall switching movie analyzed to generate the plot in Fig. 5. Also, three specific cumulative poling times (800, 1900, and 3000 ns) are identified for later discussion.

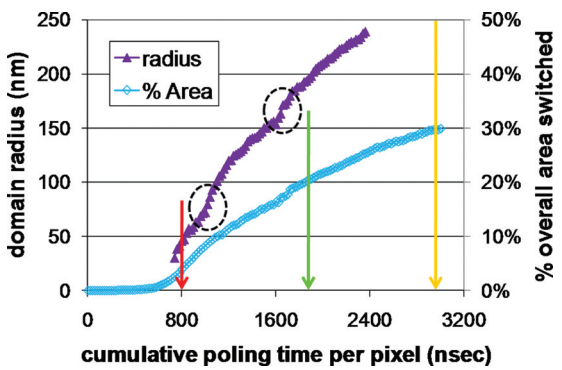

FIG. 5. (Color online) Average domain radius calculated for the single domain highlighted in Fig. 4 (left axis), with total percentage area switched superimposed (right axis), including markers for poling times of 800, 1900, and 3000 ns along with highlighted regions where the single domain radius accelerates or decelerates.

V. DOMAIN DYNAMICS CORRELATED WITH MECHANICAL COMPLIANCE

Carefully comparing the nonlinear expanding domain radius in Fig. 5 with the actual images from Fig. 4 (or the movies available online), it appears that the nonlinearities correlate with image frames that exhibit highly directional expansion and/or halting of the domain walls, presumably related to the inhomogeneous energy landscape. To further investigate this effect, the region considered for Figs. 4 and 5 was actually initially imaged with atomic force acoustic microscopy (AFAM), an AFM- based technique that allows the local mechanical compliance to be mapped by combining AFM and acoustic techniques.[21–29] In this method, the contact resonance for stiff regions occurs at a higher frequency than for compliant regions, typically appearing with bright or dark contrast respectively in AFAM images as sketched in Fig. 6(a). This contact resonance is typically mapped by monitoring the lever amplitude while sweeping frequency at every pixel,[27,30] sweeping through frequencies in a frame by frame manner and then mining the amplitude data for resonant peaks,[21] or using a resonant frequency tracking scheme[31] such as the dual-frequency-resonant-tracking method employed here [Fig. 6(b)].[32] Regardless, near-surface defects, which have previously been proposed to contribute to domain switching by lowering local energy barriers,[33,34] can therefore conceivably be identified with AFAM, as such defects may modify the local mechanical properties of the film. Consequently, a correlation between AFAM results and switching dynamics is expected.

To better compare the contact resonance (stiffness) map of Fig. 6(b) with local switching dynamics, the perimeters of several growing domains from Fig. 4 are overlaid for the three equally separated time points indicated in Fig. 5. The solid outlines (red online) identify these domains after 800 ns of cumulative pulsing per pixel, dotted lines (green online) indicate those domains after 1900 n of pulsing, and dashed lines show the domain perimeters after 3000 ns of pulsing (beyond the last frame of Fig. 4, but visible in the online supplementary movies[17]). As can be seen, locations that switch first generally correlate with regions of dark (compliant) AFAM contrast, with growth seemingly preferred toward many of these compliant regions as well. The remaining area, which exhibits a relatively higher stiffness

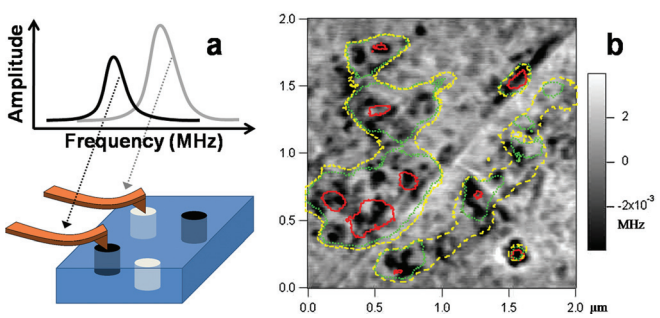

FIG. 6. (Color online) AFAM image mapping contact resonance frequency, and therefore local mechanical properties (bright = stiff, dark = compliant), for the same region as imaged in Fig. 4.

nearly everywhere, does not switch until much longer accumulated pulsing is applied (if at all).

VI. NANOSCALE DOMAIN DYNAMICS

To better quantify these observations, three distinct switching parameters are uniquely determined and presented in a single figure to reveal truly nanoscale domain dynamics. First, domain switching times are calculated based on analyzing every HSPFM phase image from the entire switching movie. Switching gradients are then calculated as described elsewhere,[35] yielding local switching directions and velocities with 14.1 nm spatial resolution based on 4×4 pixel bins. Simultaneously displaying these parameters finally generates results as shown in Fig. 7(a), which focuses on the 705×705 nm^2 region outlined by a solid square in Fig. 4. The image contrast identifies the switching time, ranging from dark nuclei to light peripheries (blue to red online) signifying switching between 720 and 2960 ns of cumulative poling; regions with black contrast did not switch at all. Vectored arrows indicate the local switching direction, from tail to head; dots instead of arrows are for pixel bins that never finished switching, typically found only at domain peripheries. The arrow length reveals the local switching velocity, ranging from more than 0.176 m/sec down to 0.014 m/sec for full magnitude to barely visible arrows (slower velocities are truncated for clarity of the substantially more numerous high speed growth vectors).

Considering Fig. 7(a) in more detail, the lower left coincides with the domain highlighted by contrast in Fig. 4 and analyzed for Fig. 5. Initially a domain wall radiates relatively uniformly away from its nucleus. As it expands toward the upper right, the domain growth predominantly veers off perpendicularly, essentially along the axis of a band sketched within the dotted ellipse. Part of the domain then passes through this region, but again strongly shunts perpendicularly as it approaches the solidly sketched area. These directional responses correspond to the two primary nonlinearities identified in the domain radius versus the cumulative switching time (Fig. 5). Separately, another domain wall converges on the solid elliptical region from the opposite direction (above right), exhibiting a similar behavior of shunting away from the sketched area.

Comparatively, Fig. 7(b) presents the mechanical compliance (AFAM contrast resonance frequency) of the same

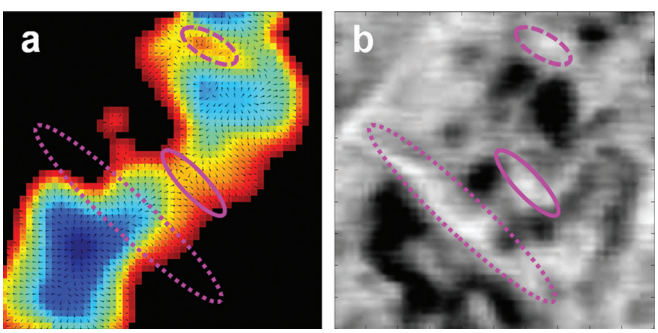

FIG. 7. (Color online) Direction-resolved dynamic switching (a) and mechanical compliance (b) of a 705×705 nm^2 region identified in Fig. 4, with the single domain tracked for Fig. 5 apparent at lower left.

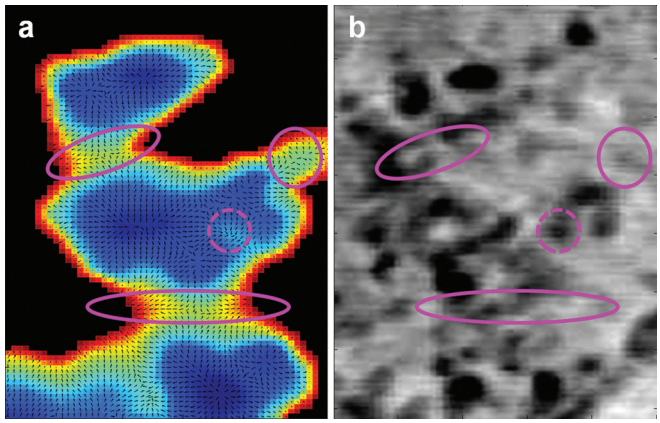

FIG. 8. (Color online) Direction-resolved dynamic switching (a) and mechanical compliance (b) for a rectangular area from Fig. 4, with several regions highlighted indicating locally nonuniform switching which correlates with local defects that influence mechanical compliance.

square area considered in Fig. 7(a), with identical sub-areas highlighted. Visualized side by side, regions that tend to nucleate first clearly correspond to dark (compliant) AFAM contrast, while regions that domains shunt around (highlighted as sketched) exhibit bright (stiff) AFAM contrast. In fact, one of the last regions to switch, only after being completely surrounded by flipped domains, is at the core of the dashed ellipse at the upper center of Fig. 7. In general, domains tend to nucleate where defects diminish the local compliance, grow toward such compliant regions (and defects) whenever possible, and conversely avoid defects which locally stiffen the sample.

Such directionally nonuniform and nonlinear domain dynamics have been regularly observed. For example, Fig. 8(a) presents the direction-resolved dynamic switching response (as with Fig. 7) for a magnified area indicated by the 847×1247 nm^2 dotted rectangle in Fig. 4. Several locations again exhibit defects according to the matched AFAM image [Fig. 8(b)], with domain wall motion either accelerated toward (dashed circle), or shunted away from (solid ellipses), compliant or stiff regions, respectively. This approach of monitoring dynamic events, mapping local nucleation and growth down to the nanoscale, and relating these properties to local mechanical compliance, topography, or other parameters (e.g., thermal, optical, electrical, and magnetic) suggests a much broader application of these methods, for example with NEMS devices, fuel cell or photovoltaic efficiency, magnetic or phase change memory devices, etc.

Notably, the specific coupling between switching and compliance observed here rules out a possible correlation between surface topography, domain switching, and compliance maps, which are always a possibility for probe-based measurements.[21] This is a concern because AFAM contrast can be enhanced at regions with higher contact area, appearing brighter, i.e., stiffer. This, in turn, would cause better tip-sample contact for ferroelectric switching,[36] and hence, should locally accelerate nucleation and growth. For instance, one of the first areas to nucleate is one of the most protruding particles, at lower right in the topography image of Fig. 4, possibly because of just such enhanced contact and

hence preferential switching. Alternatively, the apparently stiff ring around the perimeter of this protrusion (white contrast), which is a particularly common artifact for acoustic imaging, should again enhance ferroelectric switching due to the locally increased contact area, whereas domain growth essentially stalls within this ring. Likewise, the second most protruding feature from Fig. 4, nearly in the direct center of the image, does not ever switch by nucleation or growth in the acquired data even though again this would be expected to switch rapidly. Consequently, even though AFAM compliance maps and high speed SPM imaging of domain dynamics may theoretically exhibit common artifacts coupled to topographic features, for the experiments presented here, topography is essentially insignificant.

VII. CONCLUSION

By leveraging the high spatial and temporal resolution afforded by pump:probe HSPFM, ferroelectric domain dynamics have been imaged from the nascent stages of nucleation through extensive domain growth. High domain velocities for initial growth slowing beyond a roughly 100 nm radius are uniquely reported, and the repeatable nature of domain switching is clearly revealed. Most significantly, the deterministic nature of ferroelectric switching is related to local defects which influence the local mechanical compliance, modifying the energy landscape and therefore strongly influencing local and global domain growth velocities and directions. Such results have important implications for ultimate ferroelectric device densities and switching speeds, as they provide a route to measure, predict, and therefore possibly control, switching patterns and times through varying device composition, processing, and geometry. Finally, the methods employed for correlating local dynamic and mechanical properties are more broadly applicable to a variety of functional devices, such as switching in other memory elements, NEMS actuation, and energy storage.

ACKNOWLEDGMENTS

This work benefitted from funding by NSF-DMR-IMR-Development-0817263, as well as NSF- DMR-MWN-0909091.

[1]A. Gruverman, J. Mater. Sci. **44**, 5182 (2009).
[2]C. S. Ganpule, A. L. Roytburd, V. Nagarajan, B. K. Hill, S. B. Ogale, E. D. Williams, R. Ramesh, and J. F. Scott, Phys. Rev. B **65**, 014101 (2002).
[3]S. Hong, E. L. Colla, E. Kim, D. V. Taylor, A. K. Tagantsev, P. Muralt, K. No, and N. Setter, J. Appl. Phys. **86**, 607 (1999).
[4]T. Tybell, P. Paruch, T. Giamarchi, and J. M. Triscone, Phys. Rev. Lett. **89**, 097601 (2002).
[5]S. M. Yang, J. Y. Jo, D. J. Kim, H. Sung, T. W. Noh, H. N. Lee, J. G. Yoon, and T. K. Song, Appl.Phys. Lett. **92**, 252901 (2008).
[6]P. Paruch, T. Giamarchi, T. Tybell, and J. M. Triscone, J. Appl. Phys. **100**, 051608 (2006).
[7]J. F. Scott, A. Gruverman, D. Wu, I. Vrejoiu, and M. Alexe, J. Phys.:Condens. Matter **20**, 425222 (2008).
[8]J. Y. Jo, S. M. Yang, T. H. Kim, H. N. Lee, J. G. Yoon, S. Park, Y. Jo, M. H. Jung, and T. W. Noh, Phys. Rev. Lett. **102**, 045701 (2009).
[9]A. Gruverman, D. Wu, and J. F. Scott, Phys. Rev. Lett. **100**, 097601 (2008).
[10]B. D. Huey and R. Nath, in *Scanning Probe Microscopy of Functional Materials: Nanoscale Imaging and Spectroscopy*, edited by S. Kalinin and A. Gruverman (Springer, New York, 2010).
[11]N. A. Polomoff, R. Nath, J. L. Bosse, and B. D. Huey, J. Vac. Sci.Technol. B **27**, 1011 (2009).
[12]R. Nath, Y. H. Chu, N. A. Polomoff, R. Ramesh, and B. D. Huey, Appl. Phys. Lett. **93**, 072905 (2008).
[13]R. Nath, Y. H. Chu, N. A. Polomoff, P. Yu, R. Ramesh, and B. D. Huey, Nat. Nanotechnol. "High speed SPM for direct nanoscale mapping of nucleation and growth" (unpublished).
[14]R. Nath, ACS Nano "Nanoscale activation energy mapping for ferroelectric domain nucleation and growth" (unpublished).
[15]C. S. Ganpule, V. Nagarajan, H. Li, A. S. Ogale, D. E. Steinhauer, S. Aggarwal, E. Williams, R. Ramesh, and P. De Wolf, Appl. Phys. Lett.**77**, 292 (2000).
[16]N. A. Polomoff, R. N. Premnath, J. L. Bosse, and B. D. Huey, J. Mater. Sci. **44**, 5189 (2009).
[17]See supplemental material at http://dx.doi.org/ 10.1063/1.3581205 for full HSPFM phase and amplitude movies.
[18]D. J. Kim, J. Y. Jo, T. H. Kim, S. M. Yang, B. Chen, Y. S. Kim, and T. W. Noh, Appl. Phys. Lett. **91**, 132903 (2007).
[19]T. H. Kim, S. H. Baek, S. M. Yang, S. Y. Jang, D. Ortiz, T. K. Song, J. S. Chung, C. B. Eom, T. W. Noh, and J. G. Yoon, Appl. Phys. Lett. **95**, 262902 (2009).
[20]N. Balke, S. Choudhury, S. Jesse, M. Huijben, Y. H. Chu, A. P. Baddorf, L. Q. Chen, R. Ramesh, and S. V. Kalinin, Nat.Nanotechnol. **4**, 868 (2009).
[21]B. D. Huey, Annu. Rev. Mater. Res. **37**, 351 (2007).
[22]Y. G. Zheng, R. E. Geer, K. Dovidenko, M. Kopycinska-Muller, and D. C. Hurley, J. Appl. Phys. **100**, 124308 (2006).
[23]M. Kopycinska-Muller, R. H. Geiss, and D. C. Hurley, Ultramicroscopy **106**, 466 (2006).
[24]O. V. Kolosov, M. R. Castell, C. D. Marsh, G. A. D. Briggs, T. I. Kamins, and R. S. Williams, Phys. Rev. Lett. **81**, 1046 (1998).
[25]K. Yamanaka, H. Ogiso, and O. Kolosov, Jpn. J. Appl. Phys., Part 1 **33**, 3197 (1994).
[26]U. Rabe and W. Arnold, Appl. Phys.Lett. **64**, 1493 (1994).
[27]G. Stan and W. Price, Rev. Sci Instrum. **77**, 103707 (2006).
[28]J. Shin, B. J. Rodriguez, A. P. Baddorf, T. Thundat, E. Karapetian, M. Kachanov, A. Gruverman, and S. V. Kalinin, J. Vac. Sci.Technol. B **23**, 2102 (2005).
[29]D. C. Hurley, R. H. Geiss, M. Kopycinska-Muller, J. Muller, D. T. Read, J. E. Wright, N. M. Jennett, and A. S. Maxwell, J. Mater. Res. **20**, 1186 (2005).
[30]U. Rabe, S. Amelio, E. Kester, V. Scherer, S. Hirsekorn, and W. Arnold, Ultrasonics **38**, 430 (2000).
[31]R. R. Keller, D. C. Hurley, D. T. Read, and P. Rice, in *Metrologies for Mechanical Response of Micro- and Nanoscale Systems*, edited by F. Yang and J. C. M. Li (Springer, New York, 2008), p. 313.
[32]B. J. Rodriguez, C. Callahan, S. V. Kalinin, and R. Proksch, Nanotechnology **18**, 475504 (2007).
[33]S. V. Kalinin, S. Jesse, B. J. Rodriguez, Y. H. Chu, R. Ramesh, E. A. Eliseev, and A. N. Morozovska, Phys. Rev. Lett. **100**, 155703 (2008).
[34]S. V. Kalinin, B. J. Rodriguez, S. Jesse, Y. H. Chu, T. Zhao, R. Ramesh, S. Choudhury, L. Q. Chen, E. A. Eliseev, and A. N. Morozovska, Proc. Natl. Acad. Sci. U.S.A. **104**, 20204 (2007).
[35]A. Rakin, N. A. Polomoff, S. Lee, V. Palumbo, and B. D. Huey, Appl. Phys. Lett. "Resolving ferroelectric domain growth directions and velocities with sub-20 nm resolution" (unpublished).
[36]S. V. Kalinin and D. A. Bonnell, Phys. Rev. B **65**, 125408 (2002).